International Journal of Civil Engineering (2020) 18:501–518
https://doi.org/10.1007/s40999-019-00481-8

RESEARCH PAPER

RC Beam–Column Connections Retrofitted by Steel Prop: Experimental and Analytical Studies

Ali Kheyroddin[1,4,5] · Ebrahim Emami[2] · Ali Khalili[3]

Received: 19 May 2019 / Revised: 12 October 2019 / Accepted: 30 October 2019 / Published online: 15 November 2019

Abstract

This paper studies the efficiency of a proposed retrofit technique to boost the seismic behavior of beam–column connections in existing deficient reinforced concrete (RC) moment frame systems with the consideration of constraint conditions such as the height of beams, using analytical, experimental, and numerical methods. The proposed retrofit method, called the "single steel prop and curbs", consists of a diagonal steel prop element and two steel curbs that to the beam and column are laterally mounted. The internal force diagrams of the retrofitted exterior beam–column connections by analytical formulations are investigated and design strategies for promoting the efficiency of the single steel prop to achieve the expected efficiency proposed. To assay the validity and reliability of the proposed analytical procedure, experimental and numerical assessments were also conducted independently. Therefore, four deficient RC beam–column connections by single steel prop were retrofitted using three different cross-sectional areas and revival sheets and then accompanied by a control specimen subjected to cyclic loading. Next, numerical models were calibrated in ABAQUS software. Finally, by derivation of the props' average axial force from experimental and numerical results, the beam shear coefficient, β, is calculated based on the analytical relations. These results confirmed good conformity between the experimental and numerical outputs as well as reliability of the analytical formulations. Also, the output results indicated that the retrofitted specimens had 53–78% bearing capacity and 146–217% dissipated energy more than the control specimen.

Keywords RC beam–column connection · Cyclic loading · Retrofitting · Single steel prop · Steel curb

1 Introduction

Many existing reinforced concrete (RC) moment-resisting frame (MRF) structures have several deficiencies and vulnerabilities against seismic loads and need to be retrofit. Although some of the existing structures have been designed based on updated codes, there may be many practical mistakes during their construction. Contractor mistakes during construction may lead to reduced height of beams in RC frames, despite the structural analysis and design of the project. This reduced height might in turn cause undesirable performance under induced loads. Sometimes, the main aim of the reduction of height in the RC frame beams and elimination of the hanging of those in practice is to make the height of those beams uniform with the thickness of the roofs. The architectural aspects and construction feasibility are also other factors to be considered. Beam height reduction of the RC moment-resisting frames may lead to severe decrease in moment inertia,

✉ Ali Kheyroddin
kheyroddin@semnan.ac.ir; Ali.kheyroddin@uta.edu
http://www.kheyroddin.semnan.ac.ir

Ebrahim Emami
emami@se.pnu.ac.ir

Ali Khalili
a.khalili@iiees.ac.ir

[1] Faculty of Civil Engineering, Semnan University, Daneshgah Sq, Semnan 35131-19111, Islamic Republic of Iran

[2] Department of Civil Engineering, payame noor university(pnu), p.o.Box,19395-3697, Tehran, Iran

[3] International Institute of Earthquake Engineering and Seismology, Tehran, Islamic Republic of Iran

[4] University of Texas at Arlington, Texas, USA

[5] Center of Excellence for Engineering and Management of Civil Infrastructures, University of Tehran, Tehran, Iran

rigidity and strength capacity of the RC frames, so that under induced loads, vertical beams deflection and lateral displacement of those reach in excess of the allowable limit by code regulations. Based on the ATC 40 [1] procedure, after the reduction in strength and rigidity of a deficient structure, the capacity spectrum of that structure fails to intersect its demand spectrum of ground motion or by even intersecting of that the target displacement related to performance point increases remarkably. The mentioned deficiency may also lead to undesirable performance of RC beams in the serviceability state and cause cracks in joiners by escalating the vertical deflection. Therefore, to decrease the target displacement of these deficient RC frames and achieve the desired performance level of the structure under seismic and graviton forces, retrofit is needed.

Several global retrofitting methods, such as steel and concrete shear wall insertion and different types of internal and external bracing, and local retrofitting methods, such as resin injection, steel, RC and HPFRCC jacketing, steel profile and plate addition, haunch elements, external bonded FRPs and other composites, have been used for retrofitting of the deficient moment-resisting frames. Each one of these strategies can be utilized for RC frames as retrofitting targets by considering the analysis of the cost, assessment of the efficiency of operations, and architectural plausibility. Numerous researchers have used steel material in various schemes as retrofit of RC beam–column joints and local retrofitting of RC frames experimentally and numerically [2–6]. Although the main aim of these studies has been the retrofitting of RC beam–column joints, each one of the above-mentioned methods will have its own influences on RC frame performance under gravitation and seismic loads.

"Haunch retrofit solution" (HRS) as retrofit option was introduced by Yu et al. [7] following the high level of weld fractures observed at steel structures after the 1994 Northridge earthquake. Later, Chen [8] and Pampanin et al. [9] extended and designed this technique for retrofitting beam–column joints of the RC structure to shift the hierarchy of damage mechanisms to one in which the joint, as a critical component, can be protected and damage focused onto the beams. In this design model, the stiffness of the connection and the slip between the diagonal metallic haunches played a key role in the efficiency of this retrofit solution. In this regard, Eligehausen et al. [10] made numerical analyses that agreed well with the experimental results, confirming the reliability of the design approach and the experimental observations. One prohibitive requirement of the connection proposed by Pampanin et al. [9] was to use external partially pre-stressed rods to connect the haunch to the frame by drilling through holes in the slabs of the structure. To eliminate this limitation, experiments have been carried out at the joint subassembly level [11–14], as well as at the structural level [14, 15] to evaluate the performance of the so-called fully fastened haunch retrofit solution (FFHRS), where the haunch elements were connected to the frame members by using post-installed mechanical anchors. In similar cases, the HRS as a local bracing system with special orders was applied by Said and Nehdi [16], Appa Rao and Gangaram [17], Sharbatdar et al. [18, 19], Kheyroddin et al. [20], Khalili et al. [21] and other researchers. Sharbatdar et al. [18, 19] used this idea called "steel prop and curb" for rehabilitation of damaged exterior RC beam–column joints experimentally. Because of the greater satisfaction of the retrofit solution architecturally, researchers using various objects recently investigated the capability and performance of single haunch and prop element as a less-invasive retrofit solution for RC frame beam–column joints [20, 22–24]. Kheyroddin et al. [20] applied a method called "single steel prop and curbs" with and without steel revival sheets on the beam for strengthening exterior RC beam–column connections experimentally. The main idea behind this technique was the use of a steel prop which acted as a fuse element; moreover, the increase in the rigidity and strength of the system resulted in the ductility and absorption of energy being upgraded. In the study by Truong et al. [22] for existing deficient exterior beam–column joints, of the various retrofit solutions such as head re-bar anchoring, CFRP wrapping, single haunch element and steel jacketing, the steel haunch element solution generally showed better performance than other retrofit solutions in terms of the bearing capacity, stiffness, and dissipated energy. Kanchana Devi et al. [23] introduced three novel techniques for seismic retrofitting of gravity load designed (GLD) exterior beam–column joints, called single haunch, straight bar and simple angle. This researcher also showed that the specimen retrofitted with a single haunch was much better than specimens retrofitted with the other two techniques, because of no premature brittle anchorage failure and shear damage and relocating of plastic hinge from the joint toward the beam. Recently, a new retrofit solution for the GLD exterior and interior beam–column joints, "buckling restrained haunch" (BRH), was suggested by Wang et al. [25]. The objectives of this study were analysis and design of a BRH to relocate plastic hinges into beams and enhance energy dissipation of the beam–column joints. The numerical and experimental results indicated that the use of BRH, by the bracing action, load redistribution between the joints and beams and providing a stable energy dissipation capacity, was satisfactory and helped achieve their objectives. Tsang et al. [24] explored analytically the feasibility of applying a single haunch element as retrofit solution for retrofitting of RC exterior beam–column joint. They by handling of the key formulations to achieve an optimal design and

investigating effects of the factors such as length of haunch (at angle 45°) on the shear demand at the joint through a case study, they presented the failure mode and their capacity enhancement. These researchers concluded that a longer haunch could lead to a better outcome. Sasmal and Nath [26] developed the formulations for a single metallic bracing system by analytical studies. They carried out experimental and numerical studies on the beam–column sub-assemblages seismic retrofitted by single haunch with materials such as steel and a super-elastic material such as shape-memory alloy (SMA). Their researches indicated that usage of the nickel–titanium SMA is more efficient than steel bracing for seismic retrofit of the beam–column sub-assemblage. In another study, Sasmal and Voggu [27] proposed a smart and efficient system as "Strut-Relieved Single Metallic Bracing System (SBS^R)" for week joint region of GLD structures. They state that this system can act as the force path by allowing by-pass from beam to column; consequently, unnecessary damage to the structure due to single bracing can be effectively avoided.

There are several advantages using the retrofit system proposed by the mentioned researchers [18–20] compared to other similar proposed retrofitting methods. No drilling in the RC beam and column is directly required to install the steel props; therefore, no damage occurs (although a portion of slab needs to be destroyed), and furthermore the steel curbs perform their role of diffusing the loads better by confining the RC members compared to the methods proposed by other researchers. The shear strength of the members at the connection point of the steel prop to the RC members is also increased.

For the first time, Kheyroddin et al. [20] experimentally evaluated the single haunch feasibility usage ("one-way steel prop and curbs") as a less-intervention retrofit option with and without beam steel revival sheets for connections with reduced beam height. They used a single steel haunch which was architecturally less invasive and act as a fuse element for upgrading the rigidity and strength as well as the ductility and absorption energy of the deficient frames.

In this paper, the retrofit solution proposed by Kheyroddin et al. [20] with three different sectional areas of steel props was applied for two-dimensional stiffening of exterior beam–column connections of existing deficient RC structures with the aforementioned deficiency (RC frames constructed with reduced beams height) at the joint sub-assembly (see Fig. 1). The main aim of this study is based on this supposal that the RC beam height in a real existing frame structure does not have the capacity strength, rigidity, and ductility to satisfy the new retrofit codes. Therefore, by improving the structure capacity, the performance point may be upgraded to the level of the newly addressed retrofit codes. Due to architectural restrictions when using the double steel prop, a single steel prop solution is herein used which not only meets the architectural requirements, but also calls for an even less-invasive retrofit intervention. Details of the suggested seismic retrofit solution for the deficient RC frame are shown in Fig. 1.

Naturally, the proposed retrofit solution similar to other retrofit methods has its own restrictions. Based on what follows, the members of the RC frames using the retrofitted joints will be subjected to higher shear forces due to their shortened length and increased stiffness. Therefore, it is necessary to consider this shortcoming in the prop design procedure, by adjusting the maximum shear demand of the RC member under earthquake effects to prevent premature failure. In the present study, internal force diagram of a retrofitted connection and also design strategies of the single steel prop to achieve special targets are explored by analytical formulations. Also, the influence of different cross-sectional areas of the steel props on the nonlinear behavior of the deficient RC beam–column connections is experimentally and numerically investigated.

2 Analytical Study

The proposed retrofit solution, "single steel prop and curbs", can be applied for both interior and exterior connections of beam to column. Based on the hierarchy of strength for design of retrofit, if the geometry (distance from the column interface, a_p, and angle θ) and the axial stiffness K_p of the steel prop are selected properly, the bending moment in the beam at the face of the column decreases considerably, and the joint panel zone will be protected from unfavorable brittle failure mechanisms. Generally, for protection of the deficient RC joints, the process design must be such that before yielding of the steel prop, a flexural plastic hinge is formed in the beam–prop connection region. Also, according to capacity design considerations, the shear failure mechanisms should be avoided in the RC members. On the other hand, in the RC frames with reduced beam height and without weak column and joint problems, by design of a fused steel prop as first line of defense against the seismic loads, also controlling of lateral displacement, the rigidity and also strength can be upgraded.

Figures 2 and 3 show the force diagrams of a single steel prop of the as-built and retrofitted connections, respectively. As shown in Fig. 3, all the formulations presented by researchers [9] for the joints retrofitted by double haunches are acceptable for the connections retrofitted by a single prop, except of the cases that follow.

If the vertical component of the prop axial force at the beam is βV_b, the horizontal component can be defined as beam axial force F_b (only through the prop region) that is equal to:

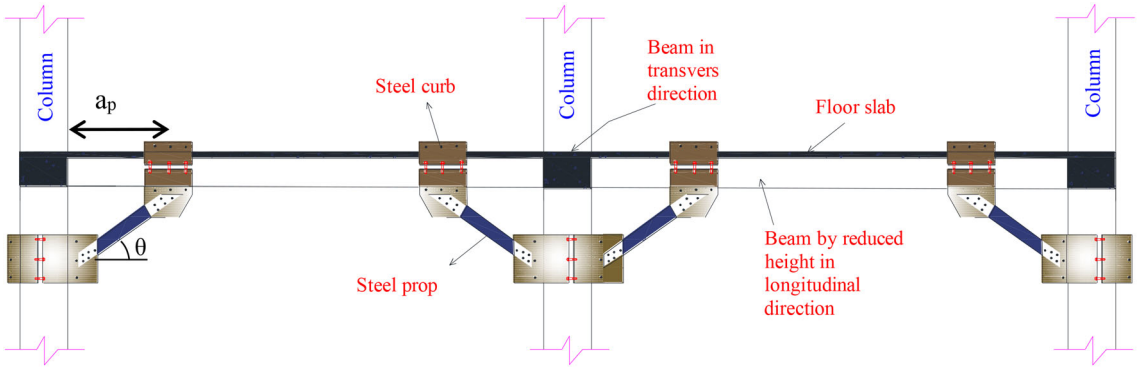

Fig. 1 Retrofitting of an RC frame with single prop solution

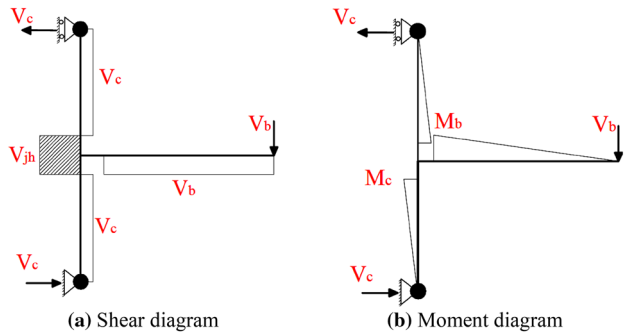

Fig. 2 Force diagrams of the exterior as-built beam–column connection

$$F_b = \beta V_b / \tan\theta. \tag{1}$$

The value of β-factor as shear transfer coefficient is derived based on displacement compatibility in the subsequent paragraph. This horizontal force F_b, with an eccentricity of $d_b/2$ due to the finite depth of the beam, produces the tensile or compressive axial force as well as concentrated moment on the beam in the prop region (at a distance of a_p from the face of the column).

In other words, until the prop is subjected to the compression force (such as the loading shown in Fig. 3), the beam at this distance acts as a beam–column member and is subjected to tensional forces and inverse. Therefore, the beam moment at the column interface, M'_b, is:

$$M'_b = V_b\left[\frac{L'_b}{2} - \frac{\beta d_b}{2\tan\theta} + (1-\beta)a_p\right], \tag{2}$$

which, according to Fig. 3b, is $\left[L'_b/2 = \left(L_n/2\right) - a_p\right]$ defined as the distance between the middle span of the beam and the location of the prop, with L_n being the net beam span length (from face to face of the columns). Since the compound of the tensile axial force and the bending moment creates the critical load combination that occurs due to the mechanism of the beam's plastic hinge at the prop region, this compound is considered in the prop design procedure. For simplicity of this procedure, the beam tensile axial force can be converted to the beam's bending moment and then added to it. As a result, by definition of a moment magnification factor of C_e, according to Eq. (3), the equivalent magnified moment, M_{eq}, is obtained. In addition, the magnification factor of C_e can approximately be obtained based on the concept of interaction diagram of the tension axial force-bending moment; therefore,

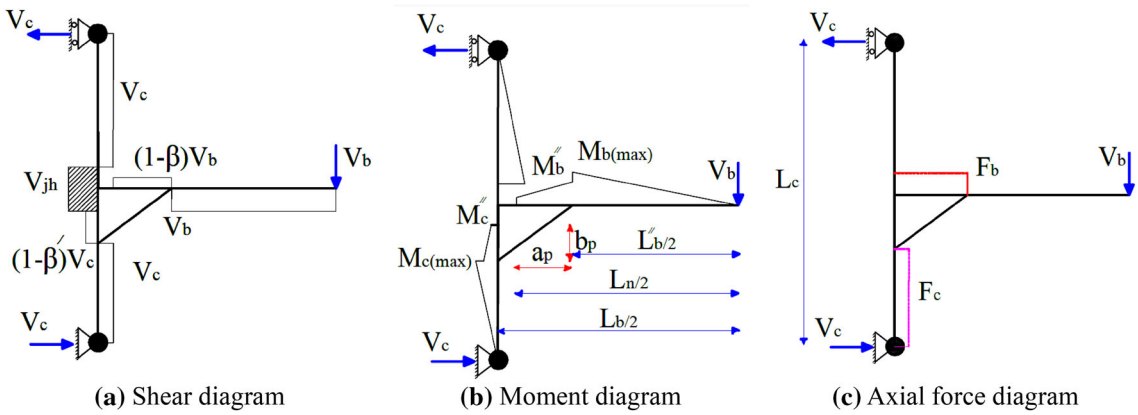

Fig. 3 Force diagrams of the exterior beam–column connection after retrofitting

$$M_{eq} = C_e \cdot M = \left(\frac{M_0}{P_0' \cdot e} + 1\right) \cdot M, \quad (3)$$

where M is the minimum value of the reduced bending moment of the RC beam at the prop region. M_0 is the bending capacity of the RC beam section without axial force. P_0' is the net tension-bearing capacity of the RC beam section and e is an equal eccentric of the bending moment (M) relative to the beam axial force (F_b) at the prop region that is derived from the following Eq. (4):

$$e = \frac{L_b' \tan\theta}{2\beta} - \frac{d_b}{2} \quad (4)$$

Equation (4) can be obtained by combining Eqs. (1) and (2), and then the ratio M/F_b can be derived from it. As illustrated above, by converting the tension axial force effect at the prop region, M_{eq} will be the base of calculations. Generally, by increasing the β-factor, the influence of axial force on the amount of M_{eq}, increases and vice versa. Moreover, by increasing the β-factor, the bending moment at the prop region will be equal to, or even bigger than, that at the outside of the prop region, (i.e., $M_{eq} \geq M_{b(max)}$) and consequently the plastic hinges can occur simultaneously in these two locations. In other words, the length of the plastic hinge at the RC beam enhancement can be confirmed. Similarly, at the prop–column connection region, due to the vertical component of the single prop axial force, a tensile/compressive axial force is produced in the column as below:

$$F_c = \beta' V_c \tan\theta = \beta V_b, \quad (5)$$

where $\beta' = \beta\left(2L_c/L_b \cdot \tan\theta\right) = \beta\left(V_b/V_c \cdot \tan\theta\right)$, with L_c the total inter-story height (from centerline to centerline of beams), L_b the total beam span length (from centerline to centerline of columns), b_p the distance from the beam interface and d_c the depth of the column. In addition, the maximum column moment developed at the level of the prop connection is:

$$M_{c(max)} = M_{b(max)} \frac{L_b L_c'}{L_c L_b'}. \quad (6)$$

Thus, as the above equations show, the steel prop axial force, F_p, especially in linear stage approximately can be estimated as follows:

$$F_p = \beta V_b / \sin\theta. \quad (7)$$

Since the applied load at the beam tip, V_b, is transferred to the column by the single prop, according to the above relation, the value of the β'-factor, like the double props, is larger than the β-factor; in other words, greater shear force is induced in the column which can be undesirable for cases where a weak column behavior is expected. For this reason, to avoid excessive increase of shear demands in the beam, and especially in column elements, it has been suggested [9] that the β-factor should not exceed a value of 2.

2.1 Estimation of β-Factor

As illustrated, the β-factor plays a key role in the reduction of beam–column interface forces. In this research, since the RC beam height was reduced and retrofitting carried out via a single steel prop, it can be expected that there was a weak beam–strong column. Moreover, the β-factor can be computed by considering the deformation compatibility between the beam (neglecting deformation of column and joint is supposed) and prop, similar to the proposed formulation by Yu et al. [7] and in accordance with the aforementioned paragraph. Therefore:

$$\beta = \left(\frac{b_p}{a_p}\right) \frac{3l_b' d_b + 3a_p d_b + 3b_p l_b' + 4a_p b_p}{3d_b^2 + 6b_p d_b + 4b_p^2 + \frac{12I_b}{A_b} + \frac{12E_c I_b}{K_p a_p \cos^2\theta}}, \quad (8)$$

where I_b and A_b are the cracked moment inertia and section area of the RC beam section, respectively, and K_p is the axial stiffness of the single steel prop.

2.2 Design Procedure of the Steel Prop

At the design stage, choosing suitable properties for the steel prop such as a_p, θ and K_p is the first step. From a practical viewpoint, especially for RC frames with the aforementioned problem (reduced beam height) and without weak column and joint problems, higher values of a_p (to decrease free beam span) and the lowest possible value of b_p (to take architectural aspects into account) should be selected for a more effective retrofit strategy. The value of K_p is also determined according to the prop element geometry and materials. It is necessary to check the axial stiffness, K_p, and yielding force of the designed steel prop to ensure that the steel prop can develop minimum vertical component $\beta_{min} V_b$ of the reaction. This vertical component can be computed by considering the deformation compatibility between the RC beam and the steel prop. β_{min} is the minimum amount of the β-factor that the plastic hinge of RC beam can form at the outside of prop region (probably at a distance of a_p from the column interface) before the yielding of the steel prop occurs.

According to Eq. (2), if the K_p of the steel prop is small (or $\beta > 1$), due to reduction of prop efficiency, it is possible that the beam plastic hinge at the column interface is formed before than where the prop is connected to beam, which is especially undesirable for the RC frames with weak columns and joints. On the other hand, according to the statements of the researchers [28], if the axial stiffness

of the steel prop, K_p, is large ($\beta < 1$) when the prop reaches its yield load, assuming it does not exhibit significant post-yielding stiffness, its efficiency in reducing the internal shears and moments in the beams and columns decreases. Moreover, the moment in the beam at the face of the column will increase at a much higher rate than it does before the prop yields (following the distribution presented in Fig. 3, without prop). Therefore, it is possible that the beam's plastic hinge at the prop–beam connection region is not formed, which can result in some damages in the beam. Consequently, in the best scenario, K_p and P_y must be selected in a way that when the prop yields, the moment of the prop–beam connection region is sufficiently close to the plastic moment of the beam ($M_{b(max)}$ or $M_{eq} = M_{by}$) to ensure that the damages on the joint and column interface do not occur before the yielding of the beam and prop. In other words, the plastic hinge can be relocated from the joint core to the prop–beam connection region before the yielding of the steel prop.

Based on the capacity design considerations, for the elastoplastic prop design of the RC frames with the aforementioned problems (reduced beam height) which have no serious problems in joints, the value of the β-factor can be computed using the following design procedure with the target energy absorption and strength in mind:

During the prop design procedure (choosing a_p, θ and K_P), the actual hierarchy of strength can be obtained by imposing that the equivalent tip beam shear corresponds to the forming of a plastic hinge in the beam and prop yielding. Herein, different states can be considered for the design of a single steel prop:

(A) for β-factor > 1.0, there are two states:

(A-1) If

$$A_p \prec \frac{F_p}{F_y} = \frac{\beta V_{b\,y-curbregion}}{F_y \sin\theta}, \tag{9}$$

where the prop yields first, then the beam moment distribution varies through length of a_p such that the beam moment at the column interface increases considerably. At this state, it is preferred that the beam's plastic hinge at the prop–beam connection region forms before or simultaneously with the interface of the column. Based on this statement, the global target hierarchy of strength and yielding of the whole design is summarized as:

$$V_{b-py} \geq \alpha_1 V_{by-curbregion}, \tag{10}$$

where α_1 is the safety factor separating the two subsequent mechanisms. The equivalent tip beam shear (sub-assembly applied lateral force) corresponding to prop yielding force, V_{b-py}, is calculated as follows:

$$V_{b-py} = \frac{A_p F_y \sin\theta}{\beta}, \tag{11}$$

where A_p is the prop section area, and F_y is the yielding stress of the steel prop. In addition, $V_{by-curbregion}$ is the equivalent of the tip beam's shear (sub-assembly applied lateral force) corresponding to the formation of the plastic hinge in the beam's curb region (or prop–beam connection region) which is given as:

$$V_{by-curbregion} = \frac{M_{b(max)}}{l'_b/2} = \frac{M_{by}}{l'_b/2}, \tag{12a}$$

Or

$$V_{by-curbregion} = \frac{M_{eq}}{\frac{l'_b}{2} - \frac{\beta d_b}{2\tan\theta}} = \frac{M_{by}}{C_e\left(\frac{l'_b}{2} - \frac{\beta d_b}{2\tan\theta}\right)}, \tag{12b}$$

where M_{by} is the yield moment of the beam.

At this state, it should be considered that although the energy absorption of the system increases, it may lead to premature rupture or buckling of the prop and the tip beam's displacement might increase remarkably in a sudden manner. Therefore, the system should be so designed that the steel prop yielding and the beam's plastic hinge at the beam curb region occur at the same time approximately, or:

$$A_p \approx \frac{F_p}{F_y} = \frac{\beta V_{by-curbregion}}{F_y \sin\theta}. \tag{13}$$

In this case, it is expectable that both the system strength and energy absorption can be increased in a controlled and desirable manner.

(i) (A-2) If the section area of the prop is sufficiently large, or

$$A_p \succ \frac{F_p}{F_y} = \frac{\beta V_{b\,y-curbregion}}{F_y \sin\theta}. \tag{14}$$

Here, the beam's plastic hinge occurs at the beam's curb region at first, and as a result depends on the value of β-factor, and both the prop's yielding and beam's plastic hinge on column interface can occur. The prop's design at this range must be such that after yielding of the steel prop, the beam at the curb region reaches its ultimate nominal bending capacity M_{bn}. In this case, the energy absorption of the system as well as its bearing capacity can be improved. Based on this statement, the global target hierarchy of

strength and yielding of the whole design can be summarized as:

$$V_{\text{b-py}} \prec \phi_1 V_{\text{b-beamhinge-int}} \prec \phi_2 V_{\text{b-collaps-curbregion}}. \quad (15)$$

Also, to ensure that the yielding of the prop occurs before the beam reaches its ultimate resistant moment, M_{bn}, at the curb region, the following capacity design requirement must be met:

$$V_{\text{b-py}} \prec \phi_1 \cdot \phi_2 V_{\text{b-collaps-curbregion}}, \quad (16)$$

where ϕ_1 and ϕ_2 are safety factors separating the two subsequent mechanisms, $V_{\text{b-beamhing-int}}$ is the equivalent of the applied tip beam shear (sub-assembly applied lateral force) corresponding to the forming of the beam's plastic hinge at the column interface which can be obtained by substituting M'_{b} with M_{by} in Eq. (2):

$$V_{\text{b-beamhing-int}} = \frac{M_{\text{by}}}{C_{\text{e}}\left(\frac{l'_{\text{b}}}{2} - \frac{\beta d_{\text{b}}}{2\tan\theta} + (1-\beta)a_{\text{p}}\right)}. \quad (17)$$

$V_{\text{b-collaps-curbregion}}$ is the equivalent of the applied tip beam shear (sub-assembly applied lateral force) corresponding to the development of the beam's ultimate nominal bending capacity, M_{bn}, at the beam's curb region.

(B) If $\frac{a_{\text{p}}}{a_{\text{p}}+\frac{d_{\text{b}}}{2\tan\theta}} \leq \beta \leq 1.0$, then the design procedure of the prop will be similar to the aforementioned process in part A.

(C) If $\beta \prec \frac{a_{\text{p}}}{a_{\text{p}}+\frac{d_{\text{b}}}{2\tan\theta}}$, then the beam's moment at the column's interface would be larger than the one at the beam's curb region; therefore, usually the prop yields and the beam plastic hinge at the interface of the column will formed.

3 Numerical and Experimental Study

A nonlinear FE analysis using ABAQUS software [29] for study behavior of the as-built and retrofitted beam–column connections was conducted. To validate the accuracy and reliability of the numerical models, the obtained results of the as-built specimen in numerical study were compared with the outputs of the control specimen DSJ experimented under cyclic loading. The force–displacement curve of the specimen DSJ obtained from the FE model was compared with the envelope hysteresis of the force–displacement response in the experiment (see Fig. 4). After making sure of the software's accuracy, the numerical analyses were conducted on the FE model DSJ, by assembly of the proposed retrofitted solution consisting of four retrofitted exterior beam–column connections named RSJ1, RSJ2, RSJ3 and RSJ4 similar to experimental specimens.

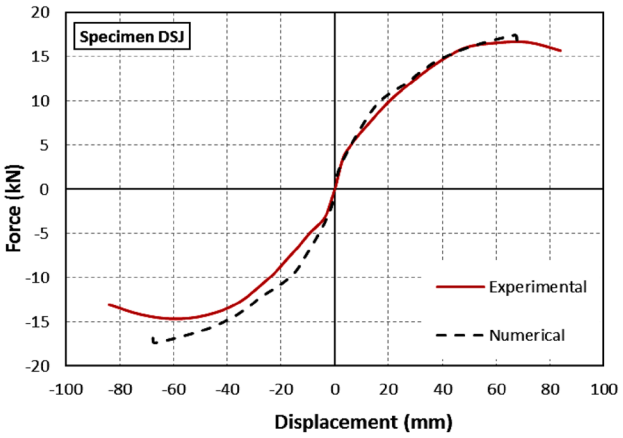

Fig. 4 Experimental and FE model force–displacement curve for as-built specimen (DSJ)

3.1 Property of Specimens

For investigation of the single steel prop performance and efficiency as a retrofit solution for RC frames with the aforementioned deficiencies under cyclic tests, four half-scaled RC exterior beam–column connections were fabricated and casted in the structural laboratory of Semnan University. For this order, an eight-story RC structure was first designed based on the middle ductility requirements of ACI 318-11 [30] and then an exterior beam–column connection at the fourth story level was opted from one of its 2-D frames. Then, to simulate the experimental specimens according to real deficient RC structures, it was supposed that during the construction process, the height 400 mm of the RC frame beams had been reduced to 300 mm due to the aforementioned limitations or practical mistakes (without variation of reinforcement details). Figure 5 and Tables 1, 2 and 3 show the geometric properties and reinforcement details of the half-scale 2-D, as-built specimen DSJ, and the retrofitted specimens RSJ1, RSJ2, RSJ3 and RSJ4. Table 4 shows also the further characteristics of the tested experimental specimens.

3.2 Test Setup and Loading Protocol

The real overview of the test setup, specimen supports, and other key components are shown in Fig. 6. As illustrated at Fig. 6, all test specimens were experimented such that by rotating them to an angle of 90° from the actual position, the column was lying horizontally and the beam vertically. The reverse cyclic load was horizontally applied under an increasing level of lateral displacement at the tip of the beam. The reverse cyclic load was applied by two 200 kN compression hydraulic jacks parallel to the column direction that were erected on the reaction frame at a distance of 1200 mm from the column face. Lateral displacement at

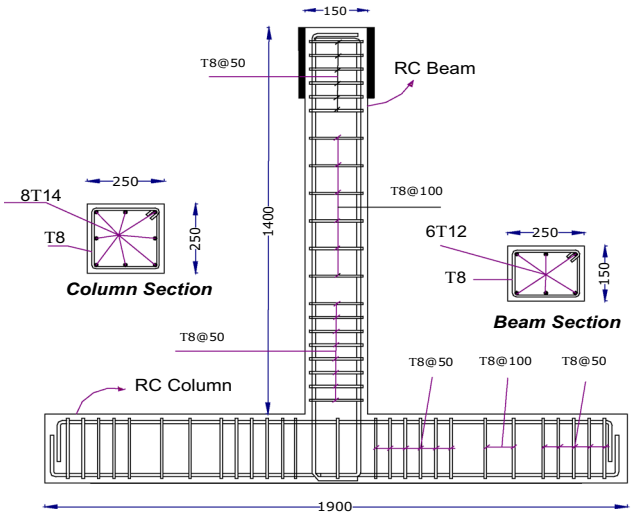

Fig. 5 Geometric properties and reinforcement details of all specimens (in mm)

Table 1 Reinforcement properties of the specimens

Member	Longitudinal reinforcement	Transverse reinforcement (in critical region)	Transverse reinforcement (noncritical region)
Beam (150 × 250 mm)	3φ 12 at Top 3φ 12 at Bot	φ 8@ 50 mm	φ 8@ 100 mm
Column (250 × 250 mm)	8φ 14	φ 8@ 50 mm (one in joint)	φ 8@ 100 mm

Table 2 Concrete compression strength

Specimen	DSJ	RSJ1	RSJ2	RSJ3	RSJ4
f_c' at 28 days (MPa)	15.5	15.3	16.0	15.0	15.7

Table 3 Mechanical properties of reinforcement bars

Bar size (mm)	Type	f_y (MPa)	ε_y (%)	F_u (MPa)	E modulus (GPa)
8	Transverse	398	0.195	586	204
12	Longitudinal	444	0.20	677	222
14	Longitudinal	510	0.22	587	232

the top of the beam was measured by two horizontal LVDTs, and two load cells were used for measuring the beam's tip reverse load. The cyclic loading history of tests, shown in Fig. 7, was based on displacement control

Table 4 Characteristics of the tested experimental specimens

Name	Specimen	Characteristics
DSJ	(As-built) control	Weak beam–column connection (with beam height equal 150 mm)
RSJ1	Retrofitted by single steel prop	Similar to DSJ, retrofitted by single steel prop (a box section with dimensions 20 × 10 × 2 mm and sectional area of A_p = 120 mm^2)
RSJ2	Retrofitted by single steel prop	Similar to DSJ, retrofitted by single steel prop (a box section with dimensions 30 × 20 × 2 mm and sectional area of A_p = 200 mm^2)
RSJ3	Retrofitted by single steel prop	Similar to DSJ, retrofitted by single steel prop (a box section with dimensions 60 × 30 × 2 mm and sectional area of A_p = 350 mm^2)
RSJ4	Retrofitted by single steel prop and revival sheet	Similar to DSJ, retrofitted by single steel prop (a box section, dimensions 30 × 20 × 2 mm and sectional area of A_p = 200 mm^2) plus steel sheets on the upper and lower surface of the beam with dimensions of 900 × 300 × 5 mm

imposed by 0.25, 0.5, 0.75, 1, 1.5, 2, 3, 4, 5, 6, 7 and 8% drifts (vertical axes shown in Fig. 7) at the tip of the beam including the double cycles at 11 steps and 24 cycles in total. Drift hereon means the relation between the beam tip displacements on the distance of the applied beam tip force from the column face.

By simulating the inflexion points at the mid-height of the columns and the midspan of the beam at a frame under lateral load, in the experimented specimens the column was supported by a hinge connection at one end and on the other end by a roller that was erected on the laboratory's strong floor. The axial load of the column was equal to $0.15P_n$ = 170 kN (P_n is nominal axial strength of RC columns) and was applied by a 500 kN hydraulic jack that together were erected with a load cell on the laboratory reaction frame (see Fig. 6).

3.3 Design of the Prop Elements and Retrofitting Method

To evaluate the influence of the prop sectional area on the behavior of the deficient RC connections, three different cross-sectionals areas based on the possible states already described in the analytical part (for β-factor > 1.0) were designed. Also, for all of the single props due to the

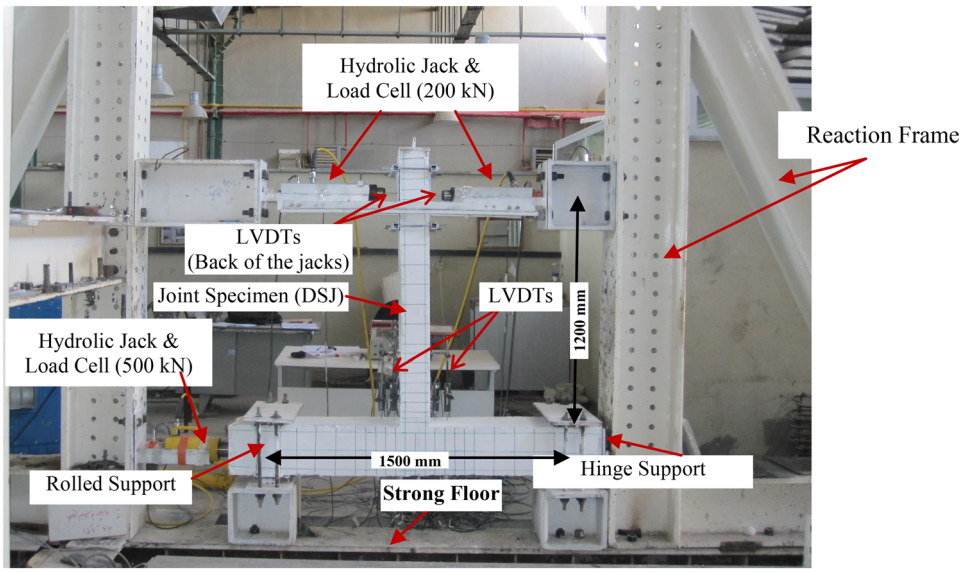

Fig. 6 General view of the test setup

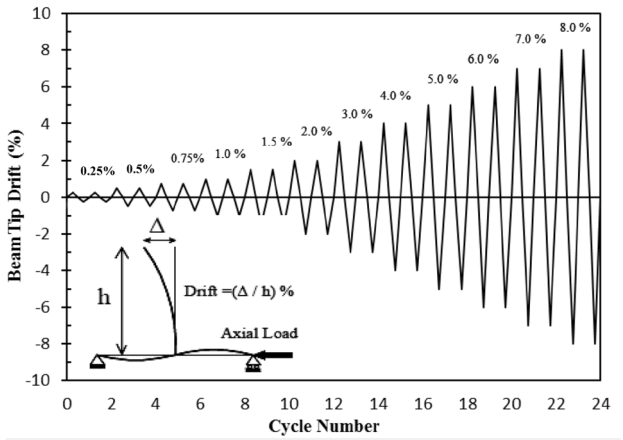

Fig. 7 Cyclic loading history of the tests

aforementioned reasons, a constant length and erection angle 500 mm and 37° were selected, respectively. The steel curbs consist of four edged L-shape plates connected and tied together to edged plates by high strength 10 mm-diameter bolts. To separate the two subsequent mechanisms, and guarantee the desired hierarchy of strength, the safety factors of $\alpha_1 = 0.9$, $\varphi_1 = 0.90$ and $\varphi_2 = 0.85$ were considered conservatively (see Table 5). The mechanical properties of different steel prop elements are also summarized in Table 6.

3.4 Experimental and Numerical Results

3.4.1 Observations of the As-Built Reference Specimen DSJ

Based on the analytical calculations and the above supposed data, the prop system consisted of the yielding fuse elements for the retrofitted specimen RSJ1, RSJ2, and RSJ4, and an elastic element for the retrofitted specimen RSJ3. The details of the retrofit solution materials and assembling of those on the beam–column connections were the same as in the published work of researchers [20]. It is worth noting that to decrease the premature buckling contingency of the steel prop, a box-shaped cross section was selected for them. The specimen DSJ, the as-built deficient beam–column connection with reduced beam height, indicated flexural behavior itself. At drift 0.25%, the beam flexural cracks were formed on the interface of the column and then those developed toward the top of the beam. The diagonal X-shape cracks in the panel zone occurred at drift 3%. From this point on, the flexural cracks were propagated on two sides of the beam length until the concrete cover at the interface of the column at drift 7% was crushed (see Fig. 8). The plotted hysteresis curve in Fig. 9 indicates a remarkable pinching that can be due to concrete weakness and the wide opening/closing of the main flexural cracks at the beam interface that caused some shear slippage of the longitudinal rebar.

3.4.2 Observations of Retrofitted Specimens

Figure 10a–d shows the final situation of the retrofitted specimens with the single steel prop system. A summary of the experimental observations are presented in Table 7.

It is worth noting that in the specimen RSJ4 for protection of the RC beam from severe damages on the upper side of the prop region and also to improve the energy absorption and rigidity of the system at the preliminary drift, the RC beam at this location was strengthened by two steel revival sheets (with dimensions of

Table 5 Expected hierarchy of strength and safety factors α_1 and φ_1 between sequence of events (design parameters: L_p = 500 mm, θ = 37°, α_1 = 0.9, φ_1 = 0.90 and φ_2 = 0.85)

Specimen	β-factor	Prop performance	V_{b-py} (kN)	$V_{by-curbregion}$ (kN)	$V_{b-beamhinge-int}$ (kN)	$V_{b-collaps-curbregion}$ (kN)	$\frac{V_{b-py}}{V_{by-curbregion}}$ $(\geq \alpha_1)$	$\frac{V_{b-py}}{V_{b-beamhinge-int}}$ $(\leq \phi_1)$	$\frac{V_{b-beamhinge-int}}{V_{b-collaps-curbregion}}$ $(\leq \phi_2)$	$\frac{V_{b-py}}{V_{b-collaps-curbregion}}$ $(\leq \phi_1 \cdot \phi_2)$
RSJ1	1.6	Fused	15.04	17	–	22.7	0.89	–	–	–
RSJ2	2.0	Fused	18.72	17	20.2	22.7	–	0.90	0.84	0.75
RSJ3	2.3	Not fused	29.2	17	26.2	22.7	–	***1.11***	***1.28***	***1.4***

Bold/italic means that in the hierarchy of strength, the steel prop won't be yielded

Table 6 Mechanical properties of the used steel props

Specimen	Steel grad	A_p (mm^2)	E-modulus (MPa)	F_y (MPa)	F_{py} (kN)	Equivalent axial stiffness K_p (kN/m)
RSJ1	300	120	196	330	39.6	47,000
RSJ2	300	200	210	312	62.4	84,000
RSJ3	300	350	187	320	112.2	131,000
RSJ4	300	200	195	318	63.6	78,000

Fig. 8 Final situation of the as-built specimen DSJ at drift 7%

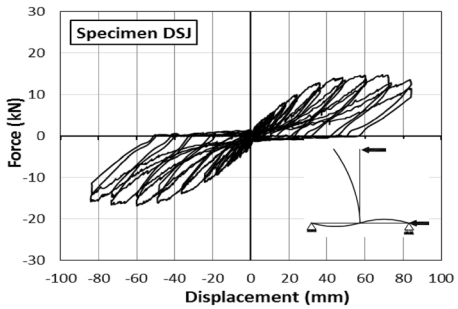

Fig. 9 Force–displacement hysteresis loop of the as-built specimen

900 × 300 × 5 mm). The steel revival sheets were attached to the RC beam by several external rods that were partially pre-stressed (see Fig. 10d). In addition, for better performance, the downsides of the sheets were welded to the upper side of the beam curb.

Figure 11 presents the force–displacement hysteresis loop of the retrofitted specimens. The hysteresis curve plotted in Fig. 11a, b for RSJ1 and RSJ2 specimens indicates that by increasing the loops area, because of the yielding in the prop and longitudinal bars, the pinching was reduced and good energy absorption (beyond 3% drift) was observed in comparison to the as-built connection. As illustrated in Fig. 11c, a stable hysteretic behavior with improved energy absorption was observed, but severe pinching still existed due to the wide opening/closing of the

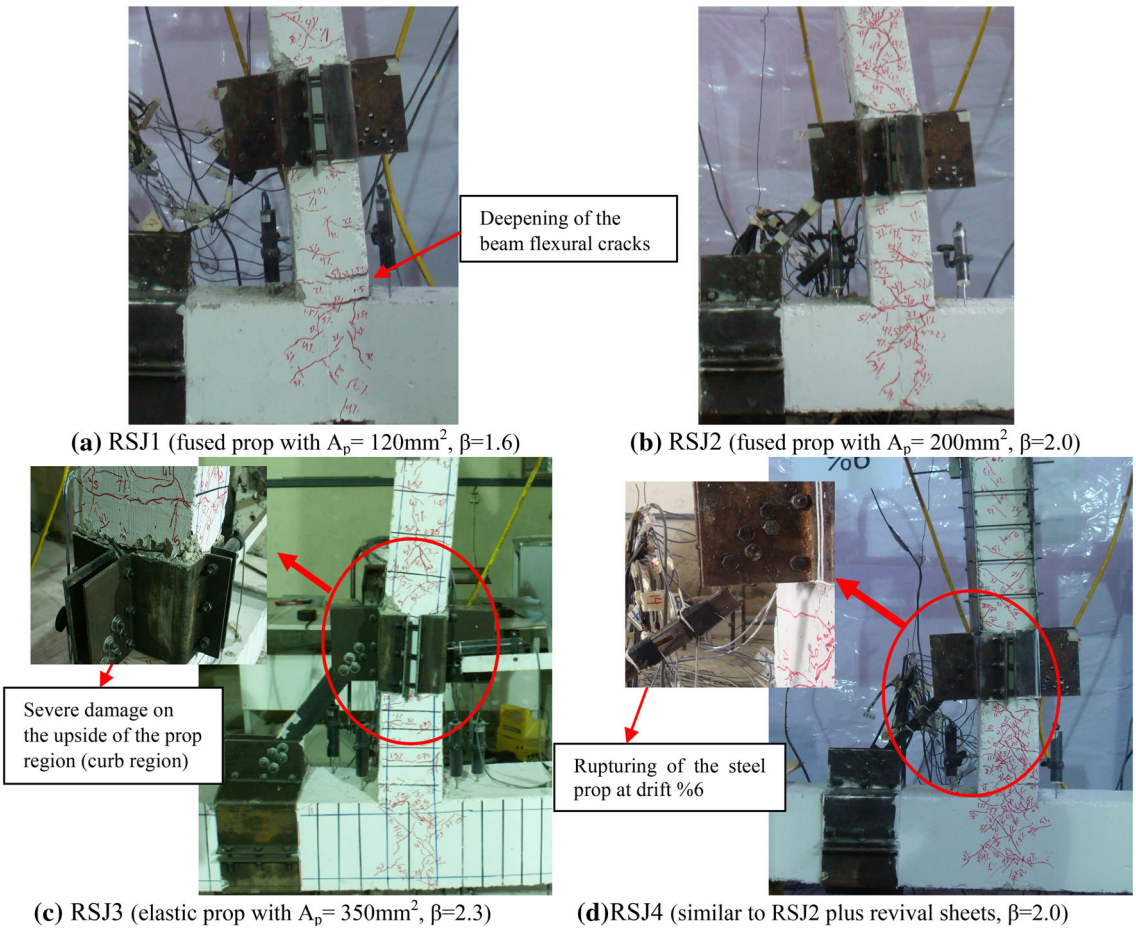

Fig. 10 Final situation of the retrofitted specimens at drift 8%

main flexural crack on the prop connection interface, which caused some shear slippage. The hysteric behavior of specimen SRJ4 indicated that by attaching the revival sheets to the single retrofitted specimen RSJ4, despite the low effect on bearing capacity, the target strength was achieved, the pinching effect was improved, and the absorbed energy increased considerably (see Fig. 11d). The force–displacement curve of each retrofitted specimen obtained from the FE model are compared with the envelope of the hysteresis load–displacement response in the test as presented in Fig. 12.

Although in the linear stage, the stiffness values of the specimens in the numerical analyses were slightly greater than the corresponding values in the experimental ones, the results obtained from the FE study are in agreement with the experimental test data. As illustrated in Fig. 12a, the opposite direction in which the steel prop was subjected to the compressive force by the whole in plane buckling of the prop bearing capacity diminution occurred. Also, for all of the retrofitted specimens in the direction in which the steel prop was subjected to compression force, the bearing capacity was more than that in the opposite direction. The envelope of the hysteresis load–displacement response presented in Fig. 12b, c indicates that there is no reduction at the bearing capacity of the FE specimen as well as the experimental specimen by the end of the test.

4 Discussion on Experimental Results

4.1 Strength of Specimens

While in the as-built specimen DSJ, the reduction of the beam's height and the weakness of concrete lead to the beam–column connection not reaching its target strength, stiffness, and absorbed energy, the opposite behavior is observed in the retrofitted specimens. As illustrated in Fig. 13, where the as-built specimen reached its maximum bearing capacity at drift 5%, the retrofitted specimens at drift 2–3% reach the same bearing capacity, which leads to the reduction of their displacement demand.

A quantitative summary of the experimental results in terms of average, maximum, and ultimate strength, initial and ultimate stiffness, and overall absorbed energy of the

Table 7 A summary of experimental observations of the retrofitted specimens

Specimens	Experimental observations
RSJ1 (fused prop with A_p = 120 mm^2, β = 1.6)	Yielding of the steel prop at drift 2.5%. Beam flexural hinging on the interface of the prop at drift 3%. Widening of a main flexural crack on the beam–column interface at drift 4% and occurring of shear cracks at the upper side of prop on the RC beam and also joint core. Buckling of the steel prop at drift 7% and progressive deepening of the beam flexural cracks in the beam–column interface. Severe buckling of the prop at drift 8%
RSJ2 (fused prop with A_p = 200 mm^2, β = 2.0)	Beam flexural hinging at the upper side of the prop region (curb region) at drift 2%. Yielding of the steel prop at drift 2.5–3%. Occurring of shear cracks at the upper side of prop on the RC beam and also joint core as well as several flexural cracks on the beam–column interface at drift 4%. Propagation of the combined shear and flexural cracks at drift 5–6%. Local buckling of the steel prop at drift 7%. Crushing of the beam concrete cover on upper side of the prop at drift 8%
RSJ3 (elastic prop with A_p = 350 mm^2, β = 2.3)	Global behavior of this specimen was rather similar to RSJ2, with the exception that the steel prop did not reach its yielding capacity. Beam flexural hinging at the upper side of the prop region at drift 2–3%. Occurring of considerable shear cracks at the upper side of prop on the RC beam at drift 5%. Progressive opening of beam's flexural cracks on the interface of the prop connection at drift 8%
RSJ4 (fused prop with A_p = 200 mm^2 plus revival sheets, β = 2.0)	Yielding of the steel prop at drift 0.5–1%. Formation of beam's flexural hinge on the inside of the prop region and interface of the column at drift 2.5%. Propagation of the pervious shear and flexural cracks and increasing number of shear cracks at the upper side of prop on the RC beam and also joint core at drift 3–5%. Rupturing of the steel prop and progressive widening of beam flexural cracks on the prop region at drift 6%

as-built and retrofitted specimens is given in Table 8, which indicates the efficiency of the proposed retrofit solution. It can be surmised that the enhanced section area of the single prop in retrofitted specimens leads to the maximum strength, 15.6 kN, in the as-built specimen and appreciably increases to values between 23.8 and 27.7 kN in the retrofitted specimens (an increase of 53–78%), without remarkable deterioration in the ultimate strength.

4.2 Stiffness of Specimens

The cyclic stiffness K_i (peak-to-peak secant stiffness) of all specimens at the every cycle is calculated using Eq. (18) and according to Fig. 14 (the hatched area). In this calculation, only the first reversal cycle is considered:

$$K_i = \frac{F_i^+ - F_i^-}{d_i^+ - d_i^-}. \tag{18}$$

The observed initial and ultimate stiffness of the retrofitted specimens (see Table 8) were from approximately 0.65 to 0.78–1.55 kN/m (an increase of 20–138%) and 0.17 to 0.17–0.32 kN/m (an increase up to 88%), respectively. It could compensate for the connection stiffness deficiency caused by the reduction in the beam height (specimen DSJ) and provide beneficial effects in limiting the excessive displacements under the lateral load also.

4.3 Energy Dissipation

The absorbed energy per cycle (E_i) is equal to the area enclosed by the complete hysteretic loop at each cycle as shown in Fig. 14. The absorbed energy per cycle for all of the specimens is presented in Fig. 15. Also, the total amount of energy absorbed ($\sum E_i$) for each specimen is obtained by calculating the area of hysteresis loops through summation [31] (see Fig. 14). The energy per cycle for the retrofitted specimens at some drifts was approximately two to four times more than the as-built specimen DSJ, as shown in Figs. 15 and 16. In addition, up to drift 6%, the retrofitted specimen RSJ4 had absorbed the most energy per cycle (about 4750 kN mm) among the specimens. Generally, the retrofitted specimens with the fused steel prop dissipated more energy except in section area of the prop, which reached high strain values. This increased dissipation of energy was as much as three times higher per cycle in the case of specimen RSJ4 compared to RSJ2 with the same section area of the prop.

As shown in Table 8, more total absorbed energy is observed in the retrofitted specimens in comparison to the as-built DSJ specimen. The difference was up to 217%, 146%, 192%, and 195% for the retrofitted specimens RSJ1, RSJ2, RSJ3, and RSJ4, respectively. Figure 16 indicates accumulative absorbed energy of the retrofitted specimens

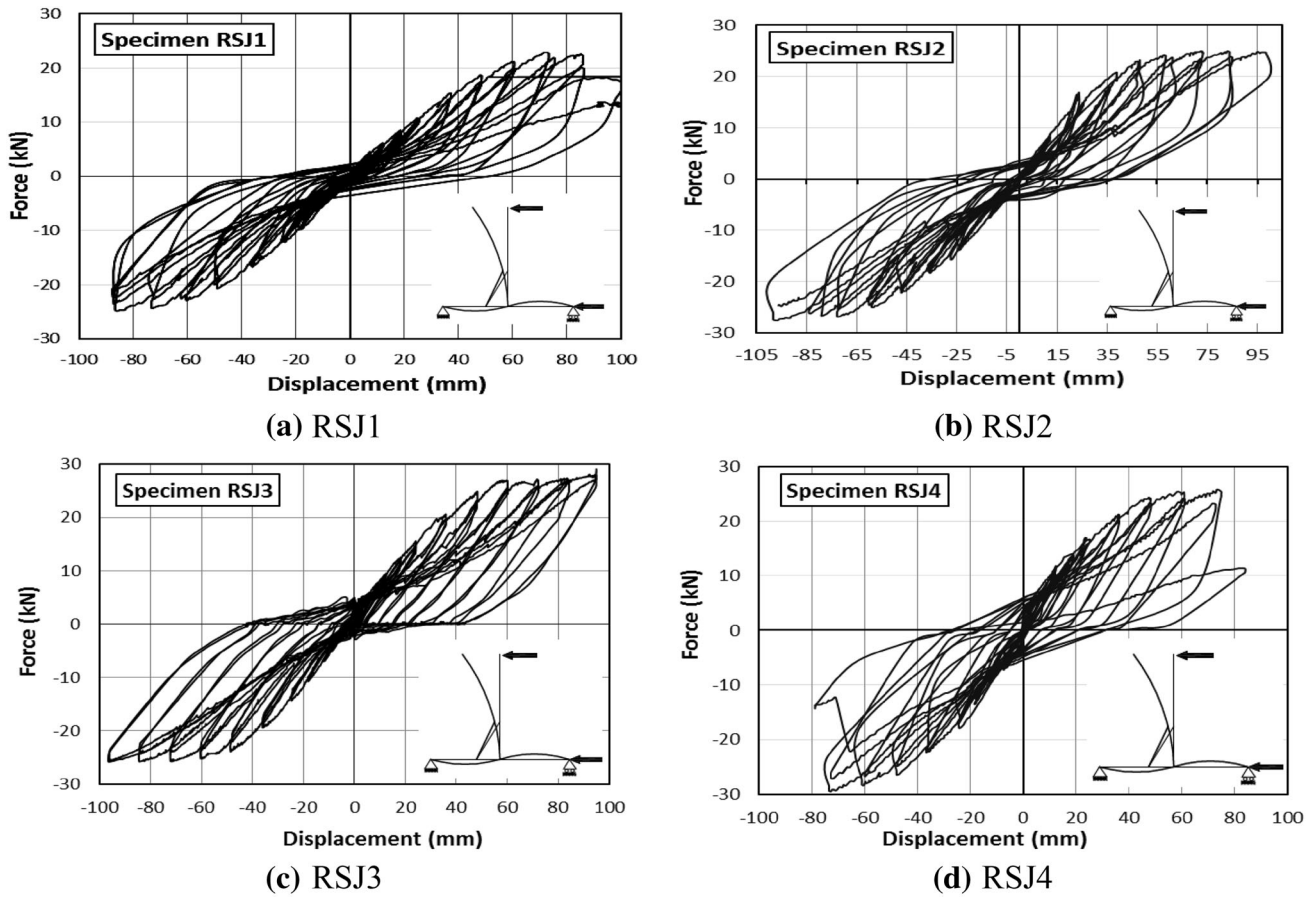

Fig. 11 Force–displacement hysteresis loop of the retrofitted specimens

in comparison to the as-built specimen DSJ at each drift. Generally, in the retrofitted specimens in which the steel prop achieved high strain values (RSJ4 > RSJ1 > RSJ2 > RSJ3) during the beam's tip loading, more accumulative energy (1–9 times) was observed compared to the as-built specimen DSJ. Therefore, it can be surmised that as the steel prop reaches its yielding load earlier, more energy is dissipated.

4.4 Damping Calculation

Damping is one of the most important parameters influencing the ability of a structure to dissipate energy under dynamic excitation. The equivalent viscous damping ratio, ξ_{eqi}, at each cycle, as illustrated in Fig. 14, can be obtained by computing the ratio of absorbed energy (E_i) to the strain energy of an equivalent linear system ($2A_e$) divided by a constant of 2π as shown in Eq. (19) [32]:

$$\xi_{eqi} = \frac{E_i}{2\pi F_i d_i} = \frac{E_i}{4\pi A_e}, \tag{19}$$

where F_i and d_i are the average peak load and displacement values for cycle i, and the area A_e represents elastic strain energy stored in an equivalent linear elastic system under static condition (dotted hatched triangle area in Fig. 14). The equivalent hysteretic damping versus drift curves for both of the as-built and retrofitted specimens are presented in Fig. 17. In this calculation, only the first reversal cycle was considered. Development of the plastic hinge length in the beam as well as yielding of the steel prop allows for a substantial improvement in the energy absorption capacity of the system, resulting in greater reduction in the displacement demand, with average equivalent viscous damping ratio, ξ_{eqi}, moving from 7.8% (during loading) to 8.4–10.2% (an increase of 8–31%).

5 Validation of the Design Procedure with Experimental and Numerical Results

Figure 18 indicates the comparison of the experimentally and numerically measured prop axial force versus the beam tip displacement for all retrofitted specimens. As shown in Fig. 18, the results obtained from the numerical study are in agreement with the experimental results regarding the prop axial force. To evaluate the validity of the suggested

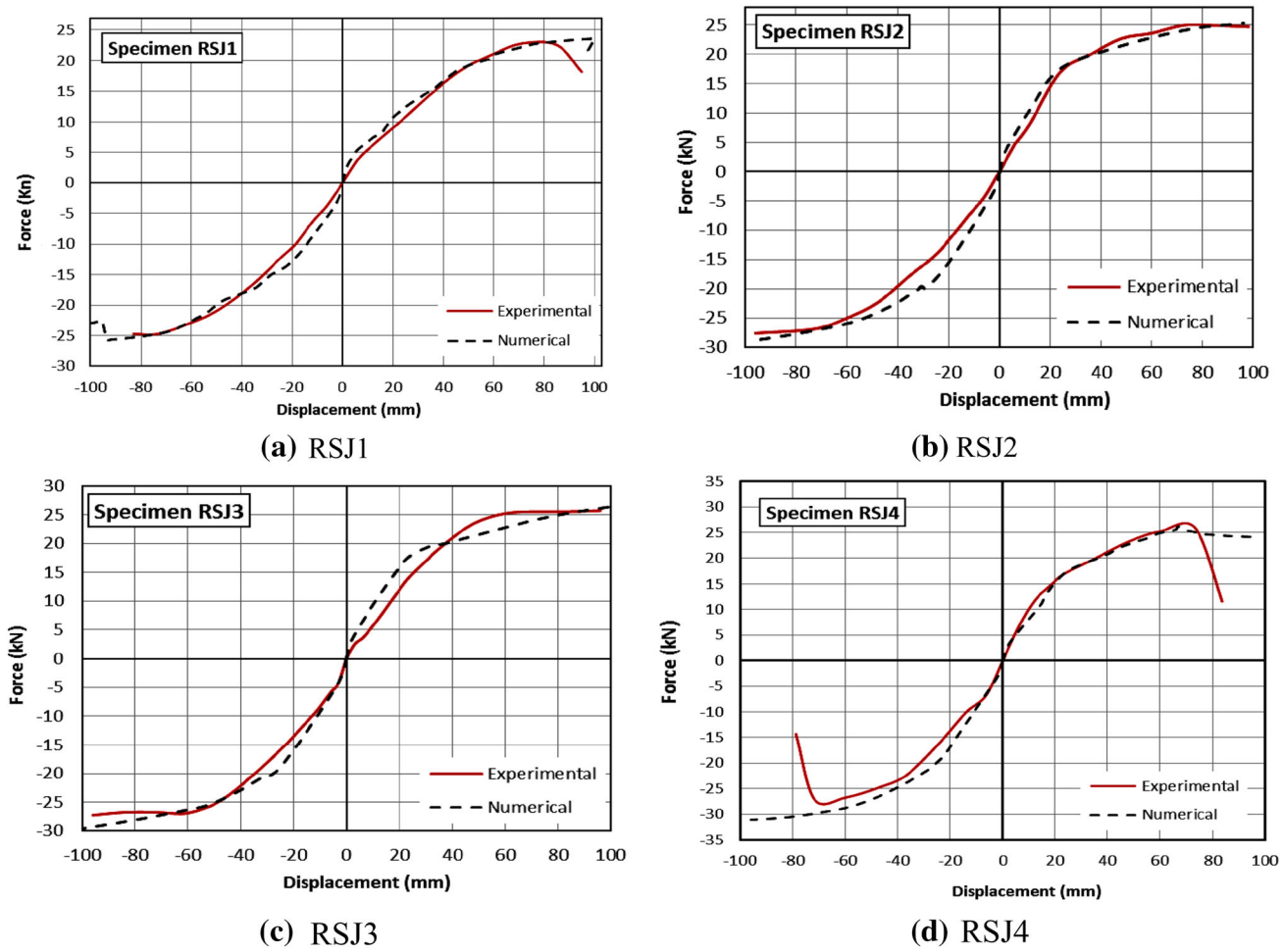

Fig. 12 Comparison of force–displacement envelope curve of FE and experimental retrofitted specimens

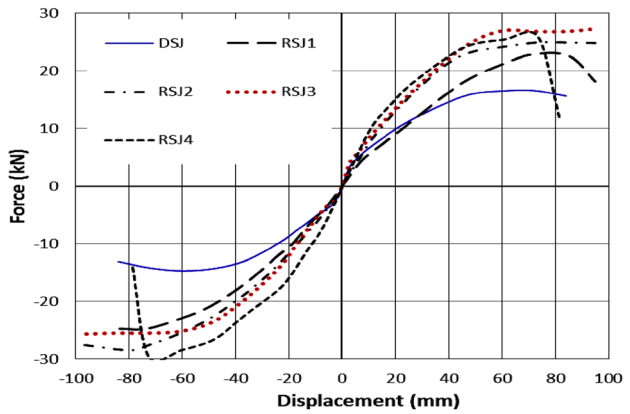

Fig. 13 Comparison of force–displacement envelope curves of the control and retrofitted specimens

analytical approach, the back-calculated responses of the retrofitted specimens are used, which are then compared to the experimentally and numerically measured responses. For the calculation of the β-factor, the formulation given in Eq. (8) also is used. In Fig. 19, the β-factors obtained from

Table 8 Summarized experimental results of as-built and retrofitted specimens

Item specimen	Ave of max strength (kN)	Ave of ultimate strength (kN)	Initial stiffness (kN/mm)	Ultimate stiffness (kN/mm)	Total absorbed energy (kN mm)
DSJ	15.6	14.6	0.65	0.17	4086
RSJ1	23.8	21.4	0.78	0.22	12,965
RSJ2	26.7	26.2	0.88	0.27	10,060
RSJ3	26.5	26.5	1.12	0.32	11,957
RSJ4	27.7	12.7	1.55	0.17	12,057

the experimental and numerical measurements are compared to the values, which were estimated using Eq. (8) and based on the properties of the tested props.

Table 9 also presents more comparisons between the analytically derived and experimental–numerical results, in terms of (i) the β-factor, (ii) the measured axial force of the

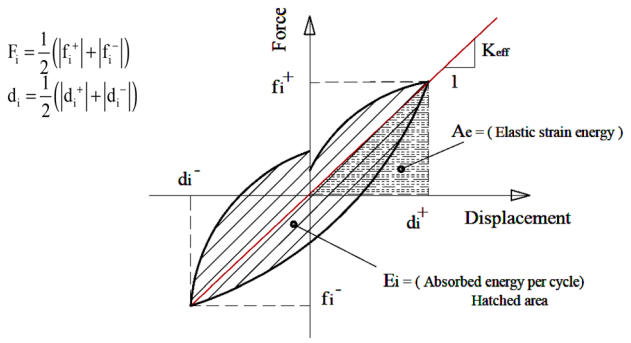

Fig. 14 Energy dissipation capacity, cyclic stiffness calculation and equivalent damping parameters

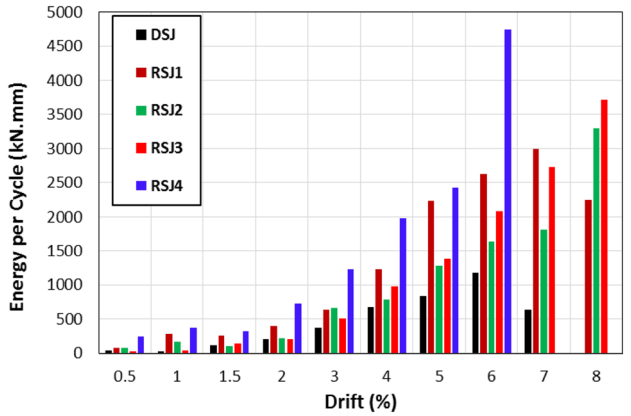

Fig. 15 Absorbed energy per cycle for all specimens

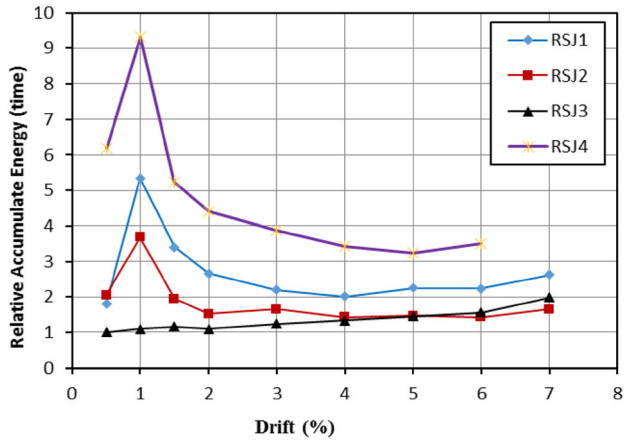

Fig. 16 Accumulative absorbed energy of the retrofitted specimens relative to as-built specimen

steel props, F_p, corresponding to development of the first mechanism event in the system, and (iii) the beam's tip lateral force corresponding to the occurrence of the first mechanism event in the system, V_b. As illustrated in Table 9, the results derived from the suggested analytical procedure are almost equal to all the measured experimental and numerical responses.

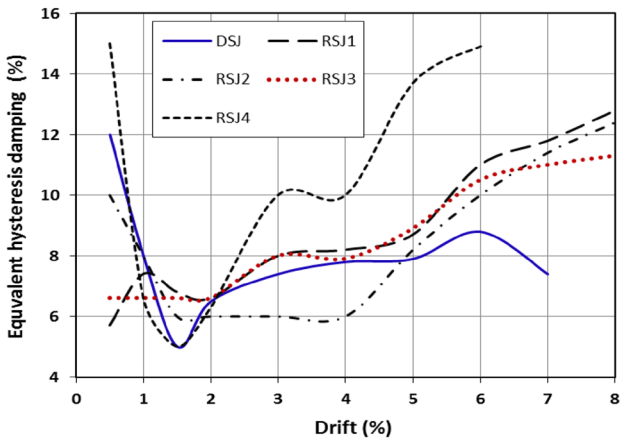

Fig. 17 Equivalent hysteresis damping ratio versus drift plot for all specimens

6 Conclusions

In the present research, the efficiency of "single steel prop" as a less-invasive solution for retrofitting of RC beam–column connections with constraint of beam height is evaluated. By analytical study and determination of internal forces of the retrofitted beam–column sub-assemblage, three steel props using various cross-sectionals areas of 120 mm^2, 200 mm^2 and 350 mm^2 (with β-factor corresponding to 1.6, 2.0, and 2.3) were designed and selected for the experimental and numerical studies. Herein, these expressions correspond to three probably occurring mechanisms as given below:

(i) The premature yielding of the steel prop and then occurrence of plastic hinge on the interface of the beam–column connection (specimens RSJ1and RSJ4).

(ii) Yielding of the steel prop simultaneously or immediately after the formation of the beam's plastic hinge on the beam–column interface or in the prop-beam connection region (specimen RSJ2).

(iii) Not yielding of the steel prop and formation of the beam plastic hinge only at the upper side of the prop–beam connection (specimen RSJ3).

The results showed good agreement between the experimental and numerical outputs in the first emerged mechanism, in terms of prop axial force as well as the beam shear coefficient, β, calculated based on the analytical formulations. The hierarchy of the occurred events in the experimental and numerical models confirmed the considered strategies for analytical design of the single steel prop.

Results investigating the experimental and numerical specimens under cyclic loading indicated that this less-

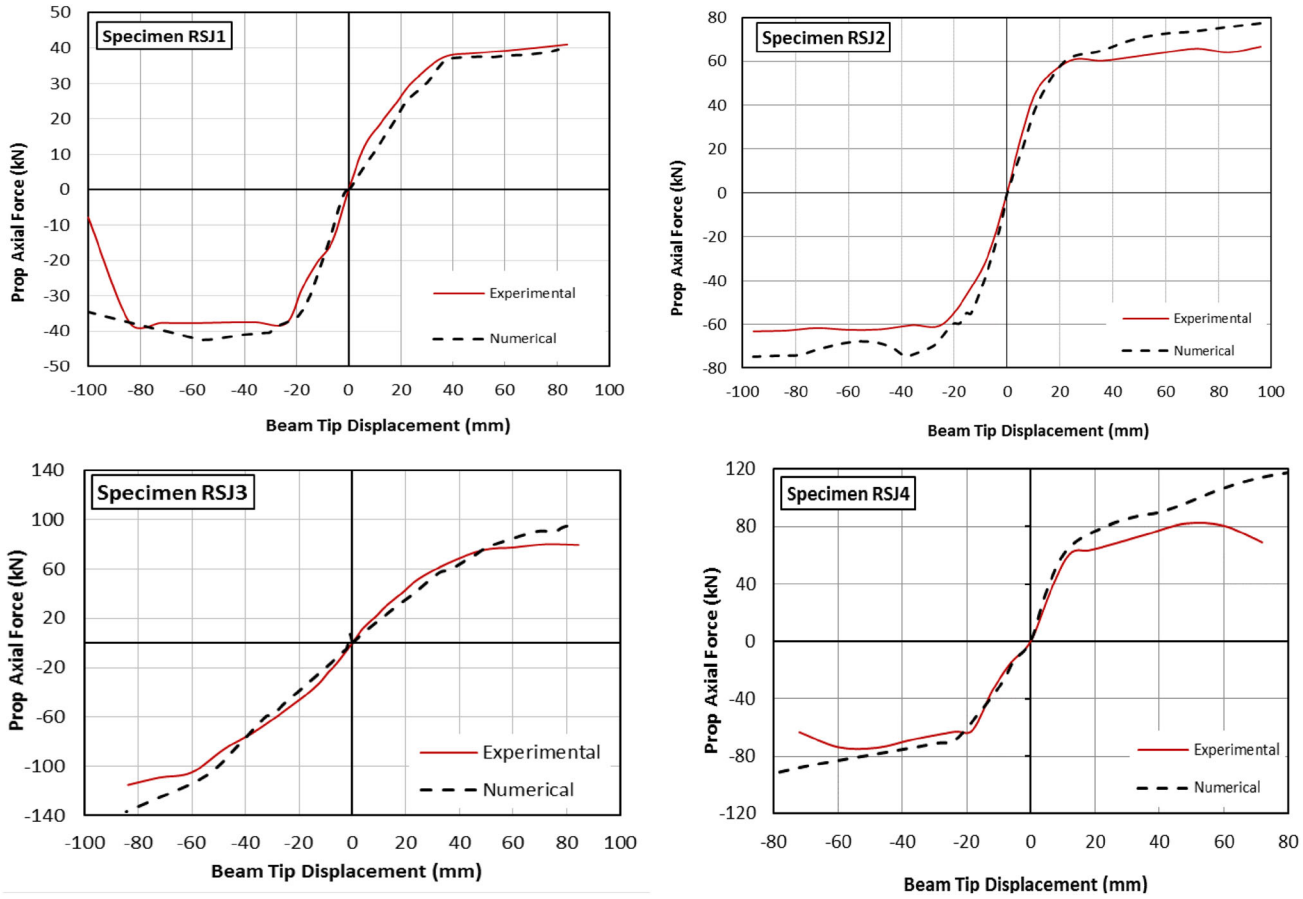

Fig. 18 Comparison of the experimental and numerical measured prop axial force versus beam tip displacement

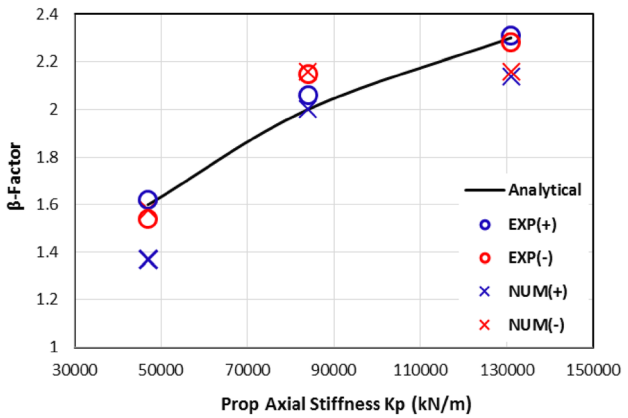

Fig. 19 Comparison of β-factors obtained from the experimental, analytical and numerical studies

invasive retrofit solution had up to 50% reduced the beam tip drift. Furthermore, using a single steel prop with low cross-sectional areas (specimens RSJ1), by creating a first defense line for system, were more energy dissipated in the system moreover providing of lateral strength and stiffness as well as the stiff steel prop (specimens RSJ3). Also, by attaching of steel revival sheets on the beam at the upper side of the beam–prop connection, the steel prop can act as a fuse element (specimens RSJ4).

The following results were also obtained by comparing the retrofitted specimens (with various section areas of the steel props of about 120–350 mm^2) to the as-built specimen up to drift 8%:

- The average of maximum bearing capacity was increased by about 1.53–1.78 times. The average of ultimate bearing capacity was increased by up to 1.82 times.
- The initial and ultimate stiffness increased by 1.2–2.39 times and up to 1.88 times, respectively.
- The total and per cycle absorbed energy were increased by about 2.46–3.17 times and up to 9.0 times, respectively. The average equivalent viscous damping ratio, ξ_{eqi}, in the as-built specimen DSJ moved from 7.8% (during loading) to 8.4–10.2% for retrofitted specimens.

Table 9 comparison results of the analytical, experimental, and numerical of the proposed retrofit strategy

Specimen	K_p (kN/m)	First mechanism			β-factor	F_p (kN)	V_b (kN)
RSJ1	47,000	Prop yielding	Analytical		1.60	39.6	14.85
			Experimental	Positive	1.62	35	13
				Negative	1.54	38	14.8
			Numerical	Positive	1.37	32	14
				Negative	1.58	40	15.2
RSJ2	84,000	Beam plastic hinge at upper side of the steel curb	Analytical		2.0	56.7	17
			Experimental	Positive	2.06	60	17.5
				Negative	2.15	61	17
			Numerical	Positive	2.0	60	18
				Negative	2.16	63	17
RSJ3	131,000	Beam plastic hinge at upper side of the steel curb	Analytical		2.3	65.2	17
			Experimental	Positive	2.31	52	13.5
				Negative	2.28	55	14.5
			Numerical	Positive	2.14	50	14
				Negative	2.14	50	14

Acknowledgements The authors would like to thank the people who financially helped them to cast and test the specimens. This research was financially supported by the Research Bureau of Semnan University.

References

1. ATC-40 (1996) Seismic Evaluation and Retrofit of Concrete Buildings, Completed by Applied Technology Council under project ATC 40, California Seismic Safety Commission, Report No. SSC 96-01, November 1996 (also available from ATC)
2. Arzeytoon A, Hosseini A, Goudarzi A (2014) Seismic rehabilitation of exterior RC beam–column joints using steel plates, angles, and posttensioning rods. J Perform Constr Facil ASCE 30(1):04014200. https://doi.org/10.1061/(asce)cf.1943-5509.0000721
3. Ruiz-Pinilla JG, Pallarés FJ, Gimenez E, Calderón PA (2014) Experimental tests on retrofitted RC beam–column joints under designed to seismic loads: general approach. Eng Struct 59:702–714
4. Santarsiero G, Masi A (2015) Seismic performance of RC beam–column joints retrofitted with steel dissipation jackets. Eng Struct 85:95–106
5. Campione G, Cavaleri L, Papia M (2015) Flexural response of external R.C. beam–column joints externally strengthened with steel cages. Eng Struct 104:51–64
6. Shafaei J, Hosseini A, Marefat MS, Ingham JM (2017) Rehabilitation of earthquake damaged external RC beam–column joints by joint enlargement using pre stressed steel angles. Earthq Eng Struct Dyn 46(2):291–316
7. Yu QS, Uang CM, Gross J (2000) Seismic rehabilitation design of steel moment connection with welded haunch. ASCE J Struct Eng 126(1):69–78
8. Chen TH (2006) Retrofit strategy of non-seismically designed frame systems based on a metallic haunch system. Dissertation, Department of Civil and Natural Resources Engineering, University of Canterbury, Christchurch
9. Pampanin S, Christopoulos C, Chen T (2006) Development and validation of a metallic haunch seismic retrofit solution for existing under-designed RC frame buildings. Earthq Eng Struct Dyn 35(14):1739–1766
10. Eligehausen R, Genesio G, Ožbolt J, Pampanin S (2008) 3D analysis of seismic response of RC beam–column exterior joints before and after retrofit. In: Alexander MG, Beushausen H-D, Dehn F, Moyo P (eds) Concrete repair, rehabilitation and retrofitting II. Taylor & Francis, London
11. Genesio G, Akgüzel U (2009) Seismic retrofit for reinforced concrete exterior beam–column joints using a fully fastened metallic haunch solution. Part 1: feasibility study—Test report, No. WS 212/23-09/02; University of Stuttgart, Stuttgart
12. Genesio G, Sharma A (2010) Seismic retrofit solution for reinforced concrete exterior beam–column joints using a fully fastened haunch. Part 2-2: retrofitted Joints, Test Report No. WS 221/08-10/02, IWB, University of Stuttgart, Stuttgart, p 136
13. Genesio G (2012) Seismic assessment of RC exterior beam–column joints and retrofit with haunches using post-installed anchors. PhD Thesis, University of Stuttgart, Stuttgart
14. Sharma A (2013) Seismic behavior and retrofitting of RC frame structures with emphasis on beam–column joints—experiments and numerical modeling. PhD Thesis, Stuttgart University
15. Sharma A, Reddy GR, Eligehausen R, Genesio G, Pampanin S (2014) Seismic response of reinforced concrete frames with haunch retrofit solution. ACI Struct J 111(1–6):1–12
16. Said A, Nehdi M (2008) Rehabilitation of RC frame joints using local steel bracing. Struct Infrastruct Eng 4(6):431–447
17. Appa Rao G, Gangaram M (2012) Non-invasive protection of shear critical non-seismically detailed RC beam–column joints against seismic loading. J Struct Eng (India) 39(3):309–317
18. Sharbatdar MK, Kheyroddin A, Emami E (2012) Cyclic performance of retrofitted reinforced concrete beam–column joints using steel prop. Constr Build Mater 36:287–294
19. Sharbatdar MK, Kheyroddin A, Emami E (2012) Experimental seismic investigation of composite RC-diagonal steel prop joints. In: Proceedings of the 15th world conference on earthquake engineering, Lisbon
20. Kheyroddin A, Khalili A, Emami E, Sharbatdar MK (2016) An innovative experimental method to upgrade performance of external weak RC joints using fused steel prop plus sheets. Steel Compos Struct 21(2):443–460

21. Khalili A, Kheyroddin A, Farahani A, Sharbatdar MK (2015) Nonlinear behavior of RC frames strengthened with steel curb and prop. Sci Iran Int J Sci Technol 22(5):1712–1722
22. Truong GT, Dinh NH, Kim JC, Choi KK (2017) Seismic performance of exterior RC beam–column joints retrofitted using various retrofit solutions. Int J Concr Struct Mater 11(3):415–433
23. Kanchana Devi AK, Karusala R, Tripathi M, Sasmal S (2018) Novel non-invasive seismic upgradation strategies for gravity load designed exterior beam–column joints. Arch Civ Mech Eng 18:479–489
24. Tsang HH, Zabihi A, Gad EF, Wilson JL (2017) Analytical model for seismic retrofit of concrete beam–column joint using diagonal metallic haunch. In: Proceedings of world conference on advanced in structural engineering and mechanics (ASEM17), IIsan (Seoul)
25. Wang B, Zhu S, Xu YL, Jiang H (2017) Seismic retrofitting of non-seismically designed RC beam–column joints using buckling restrained haunches: design and Analysis. J Earthq Eng 22(7):1188–1208
26. Sasmal S, Nath D (2017) Seismic performance of non-invasive single brace made of steel and shape memory alloy for retrofit of gravity load designed sub-assemblages. Eng Struct 143:316–329
27. Sasmal S, Voggu S (2018) Strut-relieved single steel haunch bracing system for mitigating seismic damage of gravity load designed structures. J Struct Eng. https://doi.org/10.1061/(asce)st.1943-541x.0002167
28. Christopoulos C, Filiatrault A (2000) Non-invasive passive energy dissipating devices for the retrofit of steel structures. In: Proceedings of the international conference on the behaviour of steel structures in seismic areas-STESSA 2000, Montreal, pp 387–394
29. SIMULIA (2010) Abaqus analysis user's manual. Version 6.10, Dassault Systèmes Simulia Corp. ABAQUS/STANDARD Software Help, Version 6.10.1
30. ACI 318 (2011) Building code requirements for structural concrete and commentary. American Concrete Institute, Farmington Hills
31. Priestley MJN, Mac Rae GA (1996) Seismic tests of precast beam-to-column joint sub-assemblages with un-bonded tendons. PCI J 41:64–81
32. Priestley MJN, Seible F, Calvi GM (1996) Seismic design and retrofit of bridges. Wiley, New York